Imaging Electroluminescence from Individual Nanoparticles in an Array Exhibiting Room Temperature Single Electron Effect

Jason Kee Yang Ong,[†,§] Chieu Van Nguyen,[†,§] Sena Sayood,[⊥] and Ravi F. Saraf[†,‡,*]

[†]Department of Chemical and Biomolecular Engineering and [‡]Nebraska Center for Materials and Nanoscience, University of Nebraska—Lincoln, Lincoln, Nebraska 68588, United States. [§]These authors contributed equally to the study. [⊥]Present address: University of Nebraska Medical Center, Omaha, Nebraska 68198.

ABSTRACT Electroluminescence (EL) from the monolayer of a network of a one-dimensional (1D) necklace of 10 nm Au particles (nano)cemented by CdS is imaged. The EL and photoluminescence (PL) spectra confirm the emission from CdS. The EL emission blinks and is highly specular. The position of the speckles from individual CdS cement sites is independent of magnitude and polarity of the applied bias. The EL is explained by field-assisted ionization of the cement due to high internal fields in the array caused by stationary local charging that also leads to robust single electron effect at room temperature.

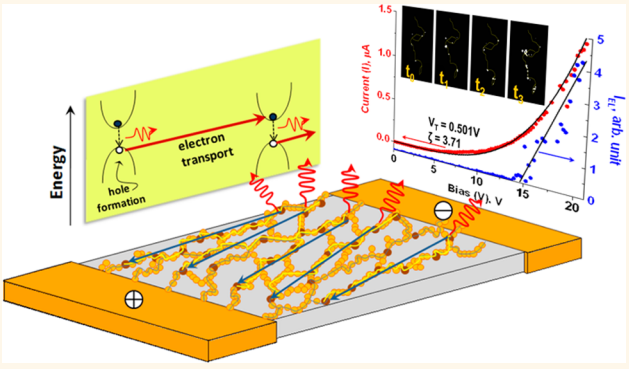

KEYWORDS: electroluminescence · nanoparticles · Coulomb blockade · single electron effect · one-dimensional nanoparticle arrays · field-assisted ionization

Electrical current through a percolating two-dimensional (2D) array of nanoparticles (NPs) as a function of applied bias is non-Ohmic. Arrays of metal nanoparticles or islands are an important class of material for their unusual electrical properties[1−3] that are similar to disordered systems, such as Luttinger liquid in carbon nanotubes[4,5] and graphene quantum dot arrays.[6] Unlike percolating arrays of microparticles, where the current (I) as a function of bias (V) has smooth nonlinear characteristics,[7] the $I-V$ of the nanoparticle array exhibits a critical threshold bias, V_T, such that $I \sim (V - V_T)^{\zeta}$, where $\zeta \sim 2$.[8−10] Simulations suggest that V_T is due to spatial distribution of quenched (*i.e.*, fixed) local charging posing a Coulomb blockade in the percolation path.[3,9] Typically, for a single 10 nm conducting particle coated with organics with a dielectric constant of $\varepsilon \sim 3$ that are present ubiquitously in the environment, the energy of the Coulomb blockade due to single electron charging is ~75 meV.[8,11] In the array, owing to multiple particles charged by a single electron in a typical percolation path between the electrodes, the net blockade barrier is greatly amplified.[3,12] However, as the temperature increases, the thermal electrons overcome the barricades successively, leading to a linear decrease in V_T as a function of T.[12,13] As a result, similar to a single NP system,[14,15] cryogenic temperatures are required to observe a robust V_T in a 2D array.[8] Recently, it was shown that, in a 1D array and a 2D network array of 1D necklaces, the V_T above a certain temperature begins to plateau.[16,17] For the necklace array system, this leads to single electron behavior at room temperature.[8,16,18]

The $I-V$ behavior is modeled analogously to a second-order phase transition with V_T being the critical point and ζ as a critical exponent.[3] The critical behavior is attributed to the random distribution of local charging at the single electron level that is stationary; that is, the location of charge centers is independent of applied bias.[3,9]

* Address correspondence to rsaraf2@unl.edu.

Received for review June 22, 2013 and accepted August 2, 2013.

Published online August 02, 2013
10.1021/nn403165q

This random quenched charge distribution over the array determines V_T and ζ. The single electron charging occurs in select particles (*i.e.*, charge centers) that are in the percolation path but isolated by a tunneling barrier from the adjacent particles with a quantum resistance larger than $\sim h/e^2 \sim 26$ kΩ, where e and h are the charge of an electron and Planck's constant, respectively.[11] The exponent, ζ, is sensitive to the tortuosity of the percolation path and the level of voids or physical defects in the 2D array.[14,19] As the number of voids increases or charge distribution becomes denser, the percolation paths become more topologically constrained, leading to a larger ζ. In an extreme case in a network of 1D necklaces of NPs, $\zeta \sim 7$ at temperature $T = 50$ K was observed.[8,18] Although experimental and simulation results are consistent with the quenched charge distribution model, a more direct signature of the (stationary) local charging has not been visualized.

Here, we report the signature of the quenched charge distribution, in a two-dimensional (2D) array of a self-assembled network of 1D Au nanoparticle necklaces by (nano) cementing the adjacent 10 nm particles with CdS and imaging the electroluminescence from individual junctions. The "nanocement" is thin enough for electron tunneling to occur. The EL also has a threshold behavior. Beyond the threshold, the EL intensity is linearly proportional to the current. The observation of EL from the array is unexpected because there is no obvious mode of hole injection in this symmetric system where the CdS cement is flanked with Au NPs on either side. The exciton formation in the necklace that causes EL is explained by a field-mediated ionization process in the cement. A key observation is the imaging of specular EL arising from discrete nanocement junctions. Consistent with the quenched charge distribution, the positions of the (blinking) speckles of EL emission are independent of polarity and magnitude of the applied bias.

RESULTS AND DISCUSSION

The necklaces are formed in the solution by bridging the negatively charged 10 nm Au particles together with Cd^{2+} bridges, as described in the Methods section. The necklace array is patterned on the chip between Au electrodes using soft lithography (see the Methods section). The local 1D nature of the array is evident in the scanning electron microscope (SEM) and transmission electron microscope (TEM) images of the monolayer of the Au(Cd^{2+})−NP necklaces on the chip and TEM grid, respectively (Figure 1a,b). The aggregation of the necklaces shown in the TEM image is attributed to the rapid solution removal during sample preparation (see Methods section). Next, the array on the chip is exposed to H_2S gas. A critical aspect of this study was the success of being able to "nanocement" the Au(Cd^{2+})−NP necklace array with H_2S gas to form CdS between the particles. The cemented necklace is designated as Au(CdS)−NP necklace arrays. Importantly, the cementing step did not affect the shape or dispersity of Au NPs. The network of Au NP necklaces appears to coalesce due to cementing as the particles

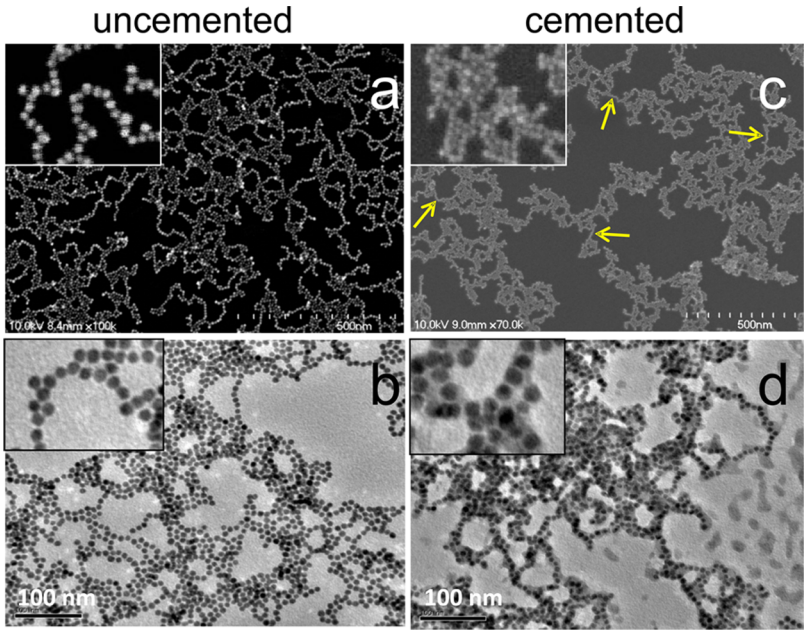

Figure 1. SEM and TEM images of Cd^{2+}-mediated Au NP necklaces before and after hydrogen sulfide treatment: (a) SEM image of Au(Cd^{2+})−NP necklace patterned on a Si chip by soft lithography. The log magnification image is shown in the Supporting Information, Figure A. (b) TEM image of the necklace array similar to (a) solution cast on a grid. (c) SEM image of the necklace after H_2S exposure. The necklaces coalesce due to CdS nanocement to form a Au(CdS)−NP necklace array. (d) TEM image of necklace similar to (c). The NPs are encapsulated by CdS cement that is clearly visible in the inset. The size of the NP is 10 nm. The coalesced clusters are connected by 1D "necklace bridges" as indicated by yellow arrows.

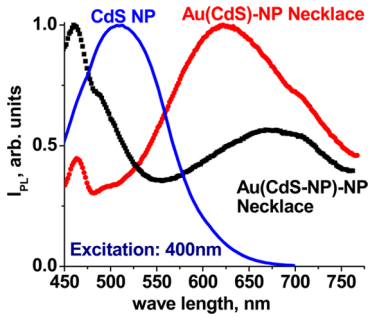

Figure 2. Photoluminescence spectra in water suspension. The PL intensity, I_{PL}, is measured for 3 nm CdS NP (blue); Au(CdS)−NP necklace (red); and Au(CdS-NP)−NP necklace (black), suspended in water. The excitation wavelength was 400 nm.

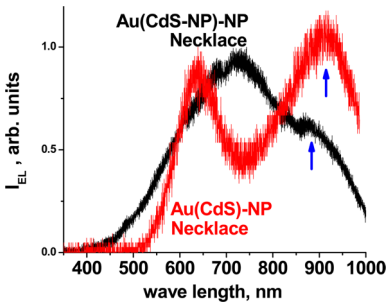

Figure 3. Electroluminescence spectra of necklace. The EL spectra for Au(CdS)−NP necklace (red) and Au(CdS-NP)−NP necklace (black) is measured on the chip at an applied bias of 20 V across a 50 μm gap between the electrodes.

move slightly to form stiffer bonds (Figure 1c). As will be discussed in Figure 2b, the coalescence does not erase the (still robust) room temperature Coulomb blockade effect. The TEM image shows that the cementing causes a formation of a thin layer that encapsulates the Au NP array (Figure 1d). The formation of inorganic CdS nanocement is confirmed by PL and EL spectroscopy, described next.

The PL spectrum of the necklace was obtained in water (Figure 2). The Au(Cd^{2+})−NP necklace suspension in water (described in the Methods section) is cemented by bubbling H_2S gas. Consistent with a previously studied Au(CdS)−NP necklace cemented by Na_2S in solution,[18] the PL spectrum shows peaks at 460 and 620 nm (red curve). The 460 nm peak is due to radiative recombination of electrons and holes in the interband transition in Au NPs.[20,21] The 620 nm peak is associated with the emissive recombination of electrons and holes mediated by an impurity state (trap) in the CdS band gap due to inclusion of Au.[18] The Au diffuses in the CdS during the formation of cement in an exothermic reaction. The exciton emission corresponding to the band gap at ~520 nm is observed for pure 3 nm CdS NPs (blue curve). Owing to the Au/CdS impurity state, the 520 nm emission is absent in the cemented necklace (red curve). The Au/CdS impurity state is further explored by making a composite necklace of CdS and Au NPs where there is no cementing involved (see Methods section). The composite necklace, Au(CdS-NP)−NP, also has the 460 nm peak due to Au NPs discussed above (black curve). The exciton peak is absent. As no Au diffusion can occur in the CdS, the 620 nm peak is also absent. However, a broad band at 675−720 nm is observed that is assigned to sulfur vacancy.[22] A similar peak as a shoulder is also observed for the Au(CdS)−NP necklace around 700 nm.

A home-built spectrometer was designed to obtain the EL spectrum (see Methods section) from the necklace array deposited on the chip and subjected to an external bias of 20 V (Figure 3). As a control, no EL was observed from the Au(Cd^{2+})−NP necklace. As expected, consistent with the assignment described above, no peak at 460 nm is observed from the Au(CdS)−NP (red curve) and Au(CdS-NP)−NP (black curve) necklaces. The peak at 640 nm in the EL spectrum for Au(CdS)−NP (red curve) is consistent with the 620 nm peak in the PL spectrum (Figure 2), supporting the assignment of an impurity level in the CdS cement due to Au diffusion. No (sharp) emission for Au(CdS-NP)−NP necklace is observed, and the 620 nm peak is absent (as expected, due to no Au impurity diffusion in CdS). The broad peak at ~700 nm in the EL spectrum for a Au(CdS-NP)−NP necklace (black curve) is consistent with the 675 nm band in the PL spectrum (Figures 2 and 3). The corresponding 700 nm peak (due to S vacancy) observed in the Au(CdS)−NP necklace in the PL spectrum was absent in the EL. This may be attributed to the dominance of the Au impurity state for the electron−hole recombination during the EL process. Additionally, a strong new peak in the near-infrared (IR) at about 900 and 850 nm for Au(CdS)−NP (red curve) and Au(CdS-NP)−NP (black curve), respectively, was observed. The origin of the IR emission is attributed to recombination of the electron in the S vacancy and the hole in the Cd vacancy.[22]

The $I-V$ characterization of the necklace was performed by applying a bias, V, in a step size of 250 mV, and the current, I, recorded was an average over three readings at each V to avoid the capacitance effect due to bias steps. The gap between the electrodes was 50 μm, and the width of the array governed by the PDMS printing was ~80 μm.[8] The $I-V$ characteristics at room temperature of Au(Cd^{2+})−NP necklace arrays indicate a strong $V_T \sim 2.0$ V (Figure 4a). The large Coulomb blockade barrier of $eV_T \sim 80$ kT makes the device very robust for room temperature operation.[11] In comparison to a dense 2D NP array, the necklace array of 50 μm has large currents and is significantly longer than a typical dense array that is usually below 2 μm.[8] The inset of Figure 4a shows the quality of the power law of $I \sim [(V - V_T)/V_T]^{\zeta}$ for the raw data. We find this plot very useful to ensure the single electron effect. The visual inspection of the linearity, especially at the lower end, is critical to consistently determine V_T.

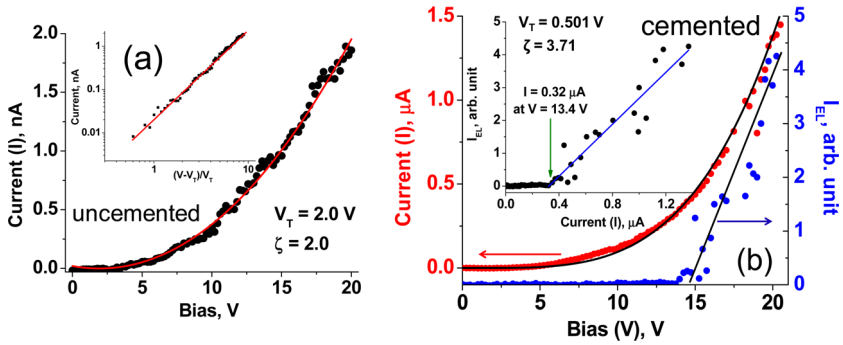

Figure 4. Electrical and electro-optical behavior of necklace array. (a) $I-V$ characteristics of Au(Cd^{2+})−NP necklace array exhibits strong nonlinear behavior with a V_T = 2 V and ζ = 2 at room temperature. The inset shows the raw data replotted in terms of reduced bias to show the scaling behavior. (b) Electrical (I) and EL (I_{EL}) behavior of the Au(CdS)−NP necklace array. Robust single electron effect with V_T = 0.5 V and ζ = 3.7 at room temperature is observed. The inset illustrates that the EL intensity, I_{EL}, is proportional to I above a threshold bias of ~13 V. The correlation to the nonlinear fit to $I-V$ for each of the plot is 0.99.

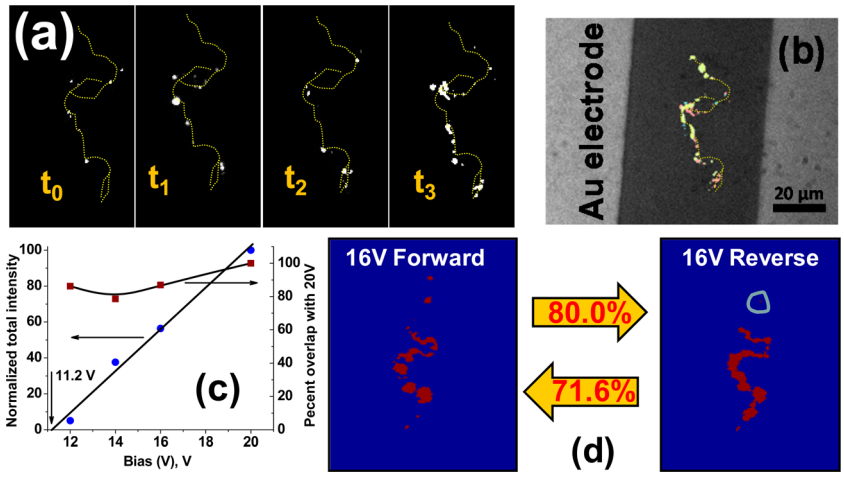

Figure 5. EL image of necklace array. (a) Raw images of EL spots at different time intervals. The contour lines are schematic to guide the eye. The image times, t_i, i = 0−3, correspond to snap shots 10 s apart. (b) Composite images made by superposing all the images acquired over 2 min at 5 s interval. (c) Parameters based on the analysis of the images. (d) Computer generated images after the analysis of the optical microscope EL images. The circled region on "16V Reverse" is to indicate the presence of an illuminated pixel.

On exposure to H_2S, the current increases by over 3 orders of magnitude; V_T decreases significantly, while ζ increases significantly (Figure 4b). The $I-V$ in Figure 4 before and after H_2S exposure is for the same sample. The increase in current during the cementing process is monitored in real time (Supporting Information, Figure B). The Coulomb blockade energy eV_T of ~20 kT at room temperature and ζ ~ 3.7 indicate robust single electron behavior at room temperature after cementing. The corresponding power law plot similar to that in the inset of Figure 4a for the cemented necklace is shown in Supporting Information, Figure C. The persistence of the Coulomb blockade observed in spite of the coalescence indicates that the array (still) has a local 1D nature; that is, the necklaces do not short to form a dense array which will completely erase the single electron behavior at room temperature.[9] The surrounding CdS cement as apparent in the TEM image (Figure 1d) prevents the shorting. However, as the chains coalesce, the number of percolation paths increases, leading to significantly larger currents. A central aspect of the morphology is the well-defined 1D necklace bridges connecting the coalesced clusters (yellow arrows in Figure 1c). The incidence of charge centers in these necklace bridges will provide an effective topological constrain to the percolation path leading to the significant Coulomb blockade observed with a robust barrier of ~20 kT. We note in passing that the significantly smaller V_T compared to necklaces cemented in solution is the low incidence of coalescence in the latter due to low concentrations of the nanoparticles.[18]

The EL threshold is significantly larger than V_T (Figure 4b, inset). The threshold is sharp and well-defined at I = 0.324 μA, corresponding to the bias of about 13.4 V. As will be confirmed below (Figure 5), no significant EL is recorded below 13 V, and the large scatter of I_{EL} is due to blinking. The electroluminescence intensity, I_{EL}, increases linearly with I (correlation parameter of ~0.89), indicating a strong correlation between the injected charge and light emission.

The EL image from a necklace array between a 50 μm gap is obtained using a highly sensitive CCD camera (Cascade II) at different time intervals (Figure 5a). The details of the setup are briefly described in the Methods section below. The contour lines on the raw images were drawn to guide the eyes to compare the location of the illumination spots between the various image frames. For a bias of 14 V, the illumination spots blink; however, their location is invariant as seen in the composite image made by superimposing over 15 (temporal) frames (Figure 5b). A simple image analysis program was developed to count the total number of illuminated pixels on the CCD camera to obtain the number and position of illuminated pixels (see Methods section). The normalized intensity, calculated as the total number of illuminated pixels relative to 20 V (the highest bias), is nominally linear with respect to bias (Figure 5c). The threshold bias to observe EL is ~11.2 V, which is reasonably consistent with Figure 4b. The smaller threshold is because the intensity by CCD is defined as the number of pixels illuminated over the whole detection area rather than total photon count. The (processed) composite images in forward and reverse bias showing the illuminated pixels above a threshold photon count indicate that over 72% of the EL spots overlap (Figure 5d). The overlap of the illuminated pixels with respect to 20 V bias image is over 80% for all biases ranging from 12 to 20 V (Figure 5c). The overlap levels and the composite images (similar to Figure 5d) for other biases are shown in Supporting Information, Figure D. Thus, the EL spots are nominally stationary with respect to bias over a large range.

The main observation of the study is the strong specular EL in the cemented necklace array that is stationary with respect to bias magnitude and direction. The observation of EL is surprising because there is no obvious hole injection process into the CdS cement to cause the electron–hole recombination. We explain the results by considering a field-assisted ionization process in the CdS cement to form the electron–hole exciton, which leads to EL on recombination. To account for the large internal fields in the array, we consider the quenched charge distribution model.

Say that α is the average number fraction of (quenched) charge centers in a percolation path with N particles between the electrodes. As the Coulomb blockade is produced by the series of capacitance of the charge centers in the path, $N\alpha \sim eV_T/E_C$, where $E_C = e^2/2C$ is the charging potential of the Au NP of capacitance C.[3,9,13,16] Assuming an average dielectric constant of the media to be ~4.2 (average of CdS (5.4) and organics (~3.5)), $C \sim 2.3 \times 10^{-18}$ F. For V_T of ~0.5 V (Figure 4b), charge center per percolation path, $N\alpha \sim 14$. (We note in passing that a 50 μm long array, with typical $N \sim 10^4$ in a percolating path, leads to $\alpha \sim 1.5 \times 10^{-3}$. The value of α is significantly smaller than 0.25 for the dense 2D array,[12] indicating that fewer charge centers in the necklace are required to block the current effectively. This topological constrain on fewer connectedness of the percolation path leads to larger ζ indicated earlier.[19,23]) A reasonable total applied potential to produce significant EL is $V = 14-20$ V (Figure 4b). If most of the potential drop occurs at the charge centers in the necklace bridges between the clusters (yellow arrows in Figure 1c), for the 50 μm gap, the average distance between the bridges should be at least ~3.5 μm. A significantly larger density of bridges at average distance of below 500 nm satisfies the high probability of charge centers at the necklace bridges (Figure 1c). Note that the model does not preclude extra (beyond the 14 needed) charge centers in the clusters. However, their effectiveness to impose a significant blockade is less because electrons can percolate around them.

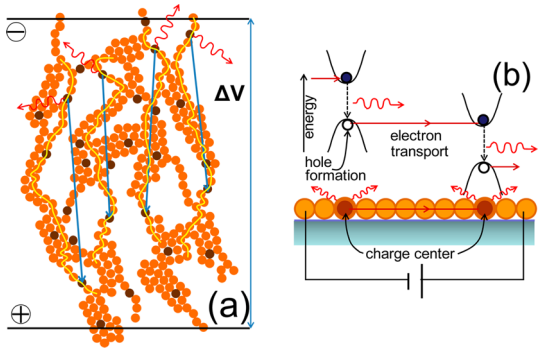

Figure 6. Model for field-assisted ionization in the necklace array for hole production. (a) Part of the network of the coalesced necklace arrays with an average potential drop of ΔV along the conduction direction. The dark shaded nanoparticle represents the stationary charged particles. The potential drop across few charged particles in the necklace bridge is ≥2.4 V, which leads to ionization (see (b)). The transport is indicated by the (four) arrow(s). A (Ohmic) conduction pathway for valence band ionization is shown in bright yellow. (b) Schematic model showing field-assisted ionization of the CdS cement. The valence and conduction band edges of CdS cement align, causing transport of an electron from the valence band (left) to the conduction band (right) *via* the coalesced cluster to generate a hole in the former. The hole subsequently recombines with an electron in the conduction band to emit a photon from the CdS cement.

A schematic of the model based on Figure 1c shows charge centers in necklace bridges and clusters (Figure 6a). The tunneling resistance, R_t, is proportional to $(V_j/16)\exp(2\beta s)$, where $\beta \sim 3.4 \times 10^9$ m^{-1} is the inverse decay length of the wave function, s is the width of the cement, and the average potential drop across each of the contacts is $V_j \sim 15V/2N\alpha \sim 100$ mV. To calculate β, a Schottky barrier between a Au/CdS (n-type) junction of ~0.65 V is assumed.[24] Due to increases in s from ~1 to ~3 nm, for good contact to charge center particle, respectively, the tunneling resistance will increase by over 7 orders of magnitude. As a result, most of the potential drop will occur across necklace bridges with the charge centers with smaller

potential gradient in the clusters. When the potential drop between two adjacent bridges is larger than 2.4 V (the band gap of CdS), ionization of the valence band will occur where the cluster will act as an "Ohmic conduit" to transport the electron (Figure 6b). The field-assisted ionization in the necklace bridge with a charge center will induce hole formation leading to EL. Such a field-assisted ionization without hole injection leading to EL has been demonstrated on a monolayer of II–VI NPs.[25,26] As there are only ~14 charge centers in a percolation path spanning between the electrodes, the incidence of such EL events for (say) 15 V bias are $\sim 14 \times 2.4V/15V \sim 2$ to 3. This explains the sparse specular EL emission spots along the percolation path in the electrode gap (Figure 5a). As the EL spots are stationary and occur due to large local potential gradient due to charge centers, the observation provides visual evidence in support of the quenched charge distribution model.

CONCLUSIONS

In summary, we have fabricated and studied a 2D array composed of a network of 1D Au NP necklaces between two Au electrodes 50 μm apart. The 10 nm Au particles are nanocemented with CdS by exposing the Cd^{2+} bridged necklace array to H_2S. The resultant structure is locally coalesced necklaces connected by 1D "necklace bridges". Three properties are observed: (i) the current in the array is enhanced by 3 orders of magnitude due to cementing with robust single electron effect at room temperature with Coulomb blockade energy, $eV_T \sim 20$ kT (*i.e.*, $V_T = 0.5$ V) and $\zeta \sim 3.7$. (ii) Although there are no hole injections from the interconnecting Au electrodes, the array exhibits strong EL from the CdS nanocement. (iii) The (blinking) EL from individual nanocemented junctions is specular where the emission spots are stationary and independent of bias magnitude and direction. The EL is explained by electric field-assisted ionization due to large internal electric fields caused by the quenched charge distribution, in particular, (single electron) charge centers in the necklace bridges. The I_{EL} commences over a bias of ~13 V and is linearly proportional to I. The EL and PL spectra are consistent, indicating that the emission is indeed from CdS cement and is dominated by defects due to diffusion of Au impurities and lattice vacancies. To our knowledge, this is the first observation of EL in a system exhibiting single electron effect at room temperature. The observation of stationary EL centers (independent of bias or polarity) is a direct proof of quenched charge distribution in NP arrays that is attributed to the single electron effect. Quenched charge distribution has been theorized for over 20 years but never directly visualized. The EL observation provides visual evidence in support of the quenched charge distribution model. The structure may provide an avenue to make solid-state lighting with planar (rather than stacked) configuration.

METHODS

Nanoparticle Necklace Array Fabrication Using Cd^{2+} Ion and CdS Nanocement (Au(Cd^{2+})–NP Necklace and Au(CdS)–NP Necklace Array). $Cd(ClO_4)_2$ solution (3.2 mM) was slowly added to 1 mL of 10 nm Au nanoparticle suspension at pH ~ 7 (BBI International) with 5.7×10^{12} particles/mL to form a necklace.[4] The formation of the necklace was evidenced by a change in color from red to blue after 12 h due to the shift in the surface plasmon resonance (SPR) band from 525 to 610 nm in the UV–vis spectrum. The shift, as discussed in the previous report,[4,14] was due to delocalization of electrons confined to a single particle to a larger number of particles in the 1D necklace.[4] The Cd^{2+} ion bridged necklace (Au(Cd^{2+})–NP necklace) was adsorbed on a SiO_2/Si chip by exposing it to the necklace suspension for 12–14 h at room temperature. The deposition occurred selectively on the patterned NH_3-plasma-modified poly(dimethyl siloxane) (PDMS) stripes described below.

The chip has the following structure. The SiO_2 passivation layer was 500 nm thick, and the 50 nm thick Au electrodes with 10 nm thick TiO_2 adhesion layer were RF sputtered through a patterned SU8 photoresist. The gap between the Au electrodes was 50 μm. Prior to PDMS, patterning the chip was cleaned in a solution mixture of acetone and 2-propanol under ultrasonic treatment for 30 min. After being vigorously washed in distilled water, the chip was exposed to Piranha solution (1:3 by volume of 50 wt % H_2O_2 and 95.0–98.0% H_2SO_4) to make its surface hydrophilic.

Subsequently, the Au(Cd^{2+})–NP necklace array was exposed to H_2S gas. The H_2S gas was generated by adding 0.5 g of sodium sulfide (from Sigma-Aldrich) to 5 mL of sulfuric acid (from Sigma-Aldrich) in a home-built "Kipps" apparatus. On exposure, the Cd^{2+} ion bridge was converted to CdS, causing nanocementing between the adjacent particles. The formation of a Au(CdS)–NP necklace array was confirmed by optical and structural measurements discussed in the text. We also noted that because H_2S is a colorless and extremely toxic gas, the experiments were conducted in a well-sealed enclosure with a H_2S monitor.

For TEM sample preparation, a drop of fresh solution (~5 μL) was casted directly on a carbon-film-coated copper (Cu) grid (from Electron Microscopy Sciences) followed by immediate removal of the excess solvent using a blotting paper. The samples were allowed to dry for ~3 h. For the Au(Cd^{2+})–NP necklace samples, the dried samples were subsequently exposed to H_2S gas in a home-built Kipps apparatus as mentioned above.

Necklace Array Fabrication Using CdS Nanoparticle Bridge (Au(CdS NP)–NP Necklace). Instead of using Cd^{2+} ions as described above, CdS NPs were used to form a necklace with 15 nm Au NPs. Positively charged CdS NPs dispersed in water solution were synthesized using $Cd(ClO_4)_2$ as the Cd source and capped with cysteamine hydrochloride, and the density was about 10^{16} particles/mL.[25] The negatively charged 15 nm Au NP suspension at pH 7 with 1.4×10^{12} particles/mL was purchased from BBI International. A mixture ratio of 1:300 of CdS NP to Au NP suspension was prepared and shaken for about 12 h to form a necklace. Similar to the above necklace, the color of the mixture changed from red to blue upon the formation of the Au(CdS NP)–NP necklace. The necklace was deposited on the chip using a procedure similar to the one described above.

Soft Lithography. PDMS (Sylgard 184) purchased from Dow Corning was used to make a stamp for microcontact printing (μCP) using a standard method.[26] A 10:1 ratio of PDMS to cross-linking agent was mixed thoroughly and degassed under vacuum for 10 min to remove unwanted microbubbles. The solution was poured on a mold with 80 μm wide lines (lithographically)

etched in a 3 μm thick photoresist (SU8). The PDMS was cured at 60 °C for 30 min and peeled off from the mold to form a stamp.

An ink was prepared by mixing a 1:1 ratio of PDMS (viscosity 1500cst) and cross-linking agent (Gelest Inc.) followed by a 25-fold dilution with hexane. The 150 μL ink solution was spin-coated at 3000 rpm for 30 s on a coverslip. The PDMS stamp was placed on the coverslip to pick up some ink. The inked stamp was placed on the chip and heated at 60 °C for 30 min. The stamp was removed, leaving a pattern of PDMS ink that had been cured due to the heating.

The 80 μm wide PDMS stripes were activated for selective deposition. The chip was exposed to NH_3 plasma at 80 W and 380 mTorr for 60 s. On exposure to plasma, the surface of the PDMS stripes was modified by amine groups. Upon dipping the chip in the solution, the negatively charged necklace from the solution deposited on the positively charged $-NH_3^+$ group formed by the NH_3 plasma treatment.

Device Characterization Methods. Absorption spectra were measured using an Ocean Optics model USB2000 spectrometer. Scanning electron microscope analysis was performed on Hitachi S4700 field-emission SEM. Transmission electron microscopy (TEM) images were obtained by a JEOL 2010 high-resolution TEM. Photoluminescence spectra of the necklace suspension were obtained by a Hitachi fluorescence spectrophotometer F-4500. Electroluminescence experiments were performed in a home-built system using Acton spectrophotometer 150 and IN/CCD-1340/100-EB/1 CCD camera to capture the spectrum. The total electroluminescence intensity data were acquired using a Hamamatsu H5784-03 photomultiplier tube (PMT). The current (I)−voltage (V) measurements were preformed in a Faraday cage using an Agilent 3458A multimeter and Agilent 6613C power supply.

Imaging Specular EL from the Array. The EL from the nanoparticle array was imaged on an optical microscope using a Cascade II CCD camera from Roper Scientific. The Cascade II CCD camera has a pixel size of 16 by 16 μm with an imaging array of 512 by 512. The quantum efficiency is more than 90%. The CCD was installed on the optical microscope with a 20× objective for a total of 200× magnification. The images were taken at a fixed bias for 2−3 min at an interval of 5 s each. This step was repeated across a range of biases (12−20 V).

Analysis of the EL Images. The images obtained are 512 by 512 in a tiff file format. The noise was filtered by removing high-frequency noise and setting the illuminated pixel cluster below a certain threshold to zero. The data were processed in Matlab. All the temporal images acquired every 5 s at fixed bias were superimposed to generate a composite image. The composite images were compared to quantitatively measure the amount of overlap between illuminated pixels. The comparison was performed for composite images at various magnitude and direction (*i.e.*, forward and reverse) of bias.

Conflict of Interest: The authors declare no competing financial interest.

Acknowledgment. R.F.S. would like to thank the Office of Basic Energy Science, DOE (DE-SC0001302) and NSF (CMMI-0926381) for financial support. About 75% of the funding is from the DOE. The authors also thank Dr. Rafal Korlacki for technical help to setup the spectrometer to obtain the EL spectrum, and Professor Khalid Sayood with help on the image analysis.

Supporting Information Available: SEM images of soft lithography patterned Au necklace array, real-time monitoring of electrical behavior of the necklace array during the cementing process, power law I−V plot of the cemented necklace, and comparison of composite EL images at various biases. This material is available free of charge *via* the Internet at http://pubs.acs.org.

REFERENCES AND NOTES

1. Geigenmuller, U.; Schon, G. Single-Electron Effects in Arrays of Normal Tunnel Junctions. *Europhys. Lett.* **1989**, *10*, 765–770.
2. Lambe, J.; Jaklevic, R. C. Charge-Quantization Studies Using a Tunnel Capacitor. *Phys. Rev. Lett.* **1969**, *22*, 1371–1375.
3. Middleton, A. A.; Wingreen, N. S. Collective Transport in Arrays of Small Metallic Dots. *Phys. Rev. Lett.* **1993**, *71*, 3198–3201.
4. Postma, H. W. C.; Teepen, T.; Yao, Z.; Grifoni, M.; Dekker, C. Carbon Nanotube Single-Electron Transistors at Room Temperature. *Science* **2001**, *293*, 76–79.
5. Bockrath, M.; Cobden, D. H.; Lu, J.; Rinzler, A. G.; Smalley, R. E.; Balents, L.; Mceuen, P. L. Luttinger-Liquid Behaviour in Carbon Nanotubes. *Nature* **1999**, *397*, 598–601.
6. Joung, D.; Zhai, L.; Khondaker, S. I. Coulomb Blockade and Hopping Conduction in Graphene Quantum Dots Array. *Phys. Rev. B* **2011**, *83*, 115323-1–115323-6.
7. Shahar, D.; Ovadyahu, Z. Dimensional Crossover in the Hopping Regime Induced by an Electric-Field. *Phys. Rev. Lett.* **1990**, *64*, 2293–2296.
8. Kane, J.; Ong, J.; Saraf, R. F. Chemistry, Physics, and Engineering of Electrically Percolating Arrays of Nanoparticles: A Mini Review. *J. Mater. Chem.* **2011**, *21*, 16846–16858.
9. Parthasarathy, R.; Lin, X. M.; Elteto, K.; Rosenbaum, T. F.; Jaeger, H. M. Percolating through Networks of Random Thresholds: Finite Temperature Electron Tunneling in Metal Nanocrystal Arrays. *Phys. Rev. Lett.* **2004**, *92*, 076801-1–076801-4.
10. Reichhardt, C.; Reichhardt, C. J. O. Charge Transport Transitions and Scaling in Disordered Arrays of Metallic Dots. *Phys. Rev. Lett.* **2003**, *90*, 046802-1–046802-4.
11. Likharev, K. K. Single-Electron Devices and Their Applications. *Proc. IEEE* **1999**, *87*, 606–632.
12. Parthasarathy, R.; Lin, X. M.; Jaeger, H. M. Electronic Transport in Metal Nanocrystal Arrays: The Effect of Structural Disorder on Scaling Behavior. *Phys. Rev. Lett.* **2001**, *87*, 186807-1–186807-4.
13. Elteto, K.; Antonyan, E. G.; Nguyen, T. T.; Jaeger, H. M. Model for the Onset of Transport in Systems with Distributed Thresholds for Conduction. *Phys. Rev. B* **2005**, *71*, 064206-1–064206-13.
14. Blunt, M. O.; Suvakov, M.; Pulizzi, F.; Martin, C. P.; Pauliac-Vaujour, E.; Stannard, A.; Rushforth, A. W.; Tadic, B.; Moriarty, P. Charge Transport in Cellular Nanoparticle Networks: Meandering through Nanoscale Mazes. *Nano Lett.* **2007**, *7*, 855–860.
15. Klein, D. L.; Roth, R.; Lim, A. K. L.; Alivisatos, A. P.; Mceuen, P. L. A Single-Electron Transistor Made from a Cadmium Selenide Nanocrystal. *Nature* **1997**, *389*, 699–701.
16. Kane, J.; Inan, M.; Saraf, R. F. Self-Assembled Nanoparticle Necklaces Network Showing Single-Electron Switching at Room Temperature and Biogating Current by Living Microorganisms. *ACS Nano* **2010**, *4*, 317–323.
17. Xu, K.; Qin, L. D.; Heath, J. R. The Crossover from Two Dimensions to One Dimension in Granular Electronic Materials. *Nat. Nanotechnol.* **2009**, *4*, 368–372.
18. Maheshwari, V.; Kane, J.; Saraf, R. F. Self-Assembly of a Micrometers-Long One-Dimensional Network of Cemented Au Nanoparticles. *Adv. Mater.* **2008**, *20*, 284–287.
19. Suvakov, M.; Tadic, B. Modeling Collective Charge Transport in Nanoparticle Assemblies. *J. Phys.: Condens. Matter* **2010**, *22*, 163201-1–163201-23.
20. Link, S.; Mohamed, M. B.; El-Sayed, M. A. Simulation of the Optical Absorption Spectra of Gold Nanorods as a Function of Their Aspect Ratio and the Effect of the Medium Dielectric Constant. *J. Phys. Chem. B* **1999**, *103*, 3073–3077.
21. Wilcoxon, J. P.; Martin, J. E.; Parsapour, F.; Wiedenman, B.; Kelley, D. F. Photoluminescence from Nanosize Gold Clusters. *J. Chem. Phys.* **1998**, *108*, 9137–9143.
22. Ferrer, I. J.; Salvador, P. Photoluminescence and Electroluminescence Mechanisms at Polycrystalline Cds in Air and in Contact with Aqueous-Electrolytes. *J. Appl. Phys.* **1989**, *66*, 2568–2577.
23. Narumi, T.; Suzuki, M.; Hidaka, Y.; Kai, S. Size Dependence of Current−Voltage Properties in Coulomb Blockade Networks. *J. Phys. Soc. Jpn.* **2011**, *80*, 114704.
24. Goodman, A. M. Evaporated Metallic Contacts to Conducting Cadmium Sulfide Single Crystals. *J. Appl. Phys.* **1964**, *35*, 573–580.

25. Bozyigit, D.; Wood, V.; Shirasaki, Y.; Bulovic, V. Study of Field Driven Electroluminescence in Colloidal Quantum Dot Solids. *J. Appl. Phys.* **2012**, *111*, 113701.
26. Wood, V.; Panzer, M. J.; Bozyigit, D.; Shirasaki, Y.; Rousseau, I.; Geyer, S.; Bawendi, M. G.; Bulovic, V. Electroluminescence from Nanoscale Materials *via* Field-Driven Ionization. *Nano Lett.* **2011**, *11*, 2927–2932.